JGR Solid Earth

RESEARCH ARTICLE
10.1029/2021JB022180

Probing the Southern Cascadia Plate Interface With the Dense Amphibious Cascadia Initiative Seismic Array

T. Alongi[1], S. Y. Schwartz[1], H. R. Shaddox[1], and D. T. Small[2]

[1]Department of Earth and Planetary Science, University of California Santa Cruz, Santa Cruz, CA, USA, [2]Department of Earth Science, University of Oregon, Eugen, OR, USA

Key Points:

- Catalog creation of 1,452 events in southern Cascadia
- Lack of shallow offshore plate interface seismicity suggests locally high coupling
- Template matching of plate interface events reveals a cluster of seismicity sensitive to long-term plate interface strain transients

Supporting Information:

Supporting Information may be found in the online version of this article.

Correspondence to:

T. Alongi,
talongi@ucsc.edu

Citation:

Alongi, T., Schwartz, S. Y., Shaddox, H. R., & Small, D. T. (2021). Probing the southern Cascadia plate interface with the dense amphibious Cascadia Initiative seismic array. *Journal of Geophysical Research: Solid Earth*, *126*, e2021JB022180. https://doi.org/10.1029/2021JB022180

Received 7 APR 2021
Accepted 17 JUN 2021

Abstract Fault coupling is vital in determining the amount of strain that is accumulated along faults. The magnitude and location of stored elastic strain energy in highly coupled regions has important implications for understanding the full range of slip behavior at plate boundary faults, as well as earthquake and tsunami hazards. We use the temporary dense amphibious array of seismometers offered by the Cascadia Initiative to create a high-resolution catalog of events to examine the spatio-temporal behavior of earthquakes near the plate interface. The data show that in southern Cascadia the plate interface updip of the geodetically locked region is nearly devoid of seismicity, therefore likely highly coupled and accumulating strain. The catalog reveals events that are clustered at the downdip edge of the highly coupled megathrust that correlate in time with nearby strain transient observations. Template matching of events in the cluster using permanent stations of the Northern California Seismic Network over a 10-year period between 2010 and 2020 indicates that this cluster is unique in space and time. Its activity only during the strain transient provides support for the utility of seismic observations in the identification of strain transients.

Plain Language Summary Great megathrust earthquakes have occurred in the Cascadia Subduction Zone. The most recent occurred in 1700, and it is expected that another will happen in the next few hundred years. Although the megathrust has hosted great earthquakes, few small interplate events have been identified along this plate boundary. Instead, a portion of the convergence between the tectonic plates is released in both periodic slow slip events and (quasi) continuous fault creep. It is essential to understand the full range of plate boundary behavior to assess the hazard risk for great earthquakes. To further this understanding, we gather data using a densely spaced temporary array of seismometers deployed in southern Cascadia in 2014–2015 to increase detection as well as determine precise earthquake locations. We identify events that are on or very near the plate boundary fault. There is some clustering of earthquakes near the plate boundary, but we find an absence of earthquakes along the shallowest segment, that indicate that the fault is likely locked. When compared to other geophysical observations in the area, it appears that the cluster of earthquakes near the plate boundary is sensitive to strain transients, demonstrating the utility of seismic observations in investigating these phenomena.

1. Introduction

Fault coupling is a critical component of the overall seismic cycle because regions of enhanced strain accumulation have frequently been spatially correlated with high coseismic slip. Relative plate motion is accommodated in earthquakes, slow slip transients, and longer term creep. The interaction of these different modes of motion are still not well understood (Walton et al., 2021). The canonical model of the subduction zone includes a highly coupled megathrust, composed predominantly of large velocity weakening asperities that are surrounded by velocity strengthening regions that may slip aseismically (Bilek et al., 2004; Lay et al., 2012). The moment of the earthquake scales with the area of slip on the fault. Cascadia has sparse seismicity and infrequent historic great earthquakes, however when great events occur, they rupture a significant area of the margin (Satake et al., 2003). It is unsurprising that in Cascadia the seismogenic section is highly coupled extending to depths of ~20 km (Hyndman, 2013; Li et al., 2018; Pollitz & Evans, 2017; Schmalzle et al., 2014). Coupling models show that the degree of coupling is spatially variable along strike, and it is thought that regions of elevated coupling are stress concentrations and have more available strain energy and could be potential nucleation sites for future earthquakes (Dieterich, 1986; Lapusta & Rice, 2003; Segall & Bradley, 2012).

The seismogenic portion of the megathrust may be bound both updip and downdip by a zone exhibiting transitional behavior of conditional stability and heterogeneity (Gao & Wang, 2017; Schwartz & Rokosky, 2007). The downdip transition zone has been shown to host spatio-temporal coincident slow slip events and tremor, known as episodic tremor and slip events (ETS) in Cascadia (Bartlow et al., 2011; Brudzinski & Allen, 2007; Dragert, 2001; Shelly et al., 2007). This model is supported by time averaged geodetic locking models that indicate that the Cascadia megathrust is less coupled at depths deeper than 20 km (Bartlow, 2020; Pollitz & Evans, 2017; Schmalzle et al., 2014). The level of updip offshore locking is poorly determined by land based Global Navigation Satellite System (GNSS) stations, and there is much uncertainty concerning the shallow updip plate interface coupling (Wang & Tréhu, 2016). The extent and magnitude of shallow coseismic slip controls tsunami excitation. The amount of updip coupling is critical in determining the absolute amount of strain accumulated along the megathrust and thus the magnitude of the impending great Cascadia earthquake.

In early 2014, southern Cascadia experienced a significant strain transient in the gap between the ETS and the highly coupled megathrust (Haines et al., 2019; Materna et al., 2019; Nuyen & Schmidt, 2021). The 2014 strain transient was observed as a rapid increase in east-ward GNSS displacements, and interpreted as a time-dependent increase in coupling (Materna et al., 2019) or the end of a long-term slow slip event that began 1.5 years prior (Nuyen & Schmidt, 2021). The precise timing of velocity changes is poorly resolved with uncertainty of several months. Improving the time resolution of such long-term strain changes may be beneficial in determining their mechanism.

Seismicity is an indicator of strain rate changes, or a perturbation to the stress field (Dieterich, 1994; Nadeau & McEvilly, 2004). This concept is demonstrated by the spatio-temporal correlation of geodetically determined slip and seismic observations of slip by tremor and near repeating earthquakes. This strong correlation has been leveraged to increase resolution and detection of smaller amplitude transient slow slip events (Bartlow et al., 2011; Bürgmann, 2018; Frank & Brodsky, 2019; Igarashi et al., 2003; Rouet-Leduc et al., 2019; Shaddox & Schwartz, 2019; Shelly et al., 2007; Uchida et al., 2020; Walter et al., 2013). It follows that if there is a change to the stress field through a strain transient (long-term slow slip event or plate interface coupling change) that it may have an observable seismic signal.

To address the outstanding scientific questions of the level of updip coupling and whether long-term strain transients can be observed seismically in southern Cascadia (Figure 1), we generate a high-resolution catalog and critically analyze events near the plate interface. We use our catalog of microseismicity to characterize the mechanical behavior of the plate interface and show that the shallow plate interface is likely highly coupled due to scarce seismicity. We also compare our catalog of plate interface seismicity to geodetic long-term strain transient observations and show a temporal correlation, providing support for the utility of seismic observations to detect and refine timing of strain transients.

2. Tectonic Setting and Data

2.1. Tectonic Background

The Cascadia Subduction Zone is in the Pacific northwest of the US and Canada. The oceanic Juan de Fuca Plate (JDF) subducts obliquely beneath the overriding continental North American Plate at a rate of 30–45 mm/yr, from the south to the north, respectively (Demets et al., 2010 or McCaffrey et al., 2007). The Cascadia trench trends approximately north-south and spans nearly 1,000 km, extending from the Queen Charlotte triple junction, offshore Vancouver Island in the north to the southern terminus at the Mendocino Triple Junction offshore Northern California. The Cascadia Subduction Zone is proximal to the spreading ridge compared to other subduction zones. It represents the warm subduction zone endmember, and as such, the JDF is young, warm, thin, and buoyant as it enters the trench. In southern Cascadia, the spreading center is closer to the trench resulting in distinct behavior. This portion of the JDF is known as the Gorda plate. The Gorda plate's dip varies near the Mendocino Triple Junction, shallowing at about 15 km and increasing again at 25 km (McCrory et al., 2012), clearly seen in the plate interface contours in Figure 1. A significant portion of Cascadia seismicity occurs in the southernmost region, within the highly deformed Gorda plate. The largest Gorda plate earthquakes occurring as strike-slip events accommodating north-south compression (Gulick et al., 2001).

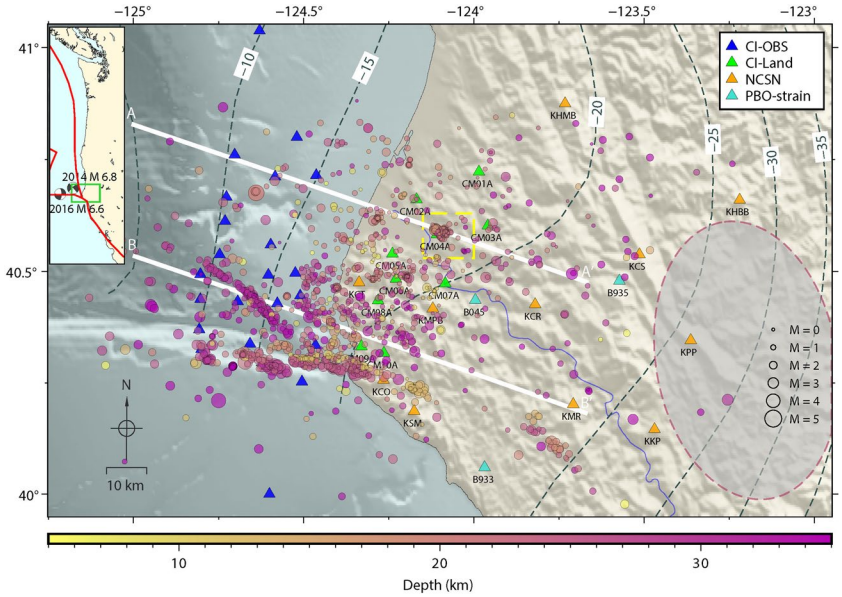

Figure 1. Regional map of the Mendocino Triple Junction area in Northern California. Inset map shows the North American west coast where the study region is indicated by the green box, plate boundaries are shown in red, and two regional earthquakes that occur outside the time of the study are indicated (see discussion Section 4.4). Main map region showing shaded relief topography and bathymetry. Plate interface contours indicated with dark dashed lines and annotation are depth to interface (McCrory et al., 2012). Earthquake locations (this study) are circles that are scaled by magnitude and colored by depth. White cross section lines as shown in Figure 2. Gray ellipse with pink dashed outline indicates area of strain transients (Materna et al., 2019; Nuyen & Schmidt, 2021). Dashed yellow box shows the Fortuna cluster. Triangles denote seismic stations used; blue for Cascadia Initiative (CI) ocean bottom seismometer, green for CI-short period land stations, and permanent Northern California Seismic Network Stations shown in orange. PBO-strain meters shown in light blue.

2.2. Data

The Cascadia Initiative (CI), a community-driven, National Science Foundation funded experiment, deployed a temporary, transportable array of onshore/offshore seismometers to understand the Cascadia Subduction Zone plate boundary (Toomey et al., 2014). Here we utilize the data from the fourth and final leg of the experiment, focused on southern Cascadia with ∼10 km seismic station spacing (Figure 1). The deployment consisted of 19, 3-component broadband ocean bottom seismometers (OBS—network code 7E) atop the continental shelf and slope recording at sampling rates between 50 and 125 Hz, depending on the instrument design. The OBS operated continuously from July 2014 to September 2015, and six of the instruments were equipped with absolute pressure gauges, though not used for this study. The onshore deployment included 11, 3-component short period instruments sampling at 100 Hz, focused near the coast, near the Mendocino Triple Junction and operated from September 2014 to September 2015 (network code 5E). Continuous waveform data from 14 permanent Northern California Seismic Network (NCSN) stations closest to the triple junction were also used throughout January 2010 to January 2020.

3. Methods & Results

3.1. Catalog Generation

3.1.1. Manual Pick and Initial Locations

We build a catalog by manually picking P-phase arrivals on continuous waveform data by visual inspection of vertical components of the seismograms. The events were initially located using the dbgenloc algorithm in Antelope (Pavlis et al., 2004) using a 1D velocity model befitting a subduction zone setting. We calculate local magnitudes within Antelope (mlrichter) and retain these magnitudes throughout the subsequent relocation steps. Manual picking of events resulted in 1,900 earthquakes identified during the deployment (July 2014–September 2015).

3.1.2. Relocation Using a 3D Velocity Model

Strong regional lateral velocity contrasts exist due to proximity to the Mendocino Triple Junction. For improved absolute locations, events were relocated using a 3D velocity model (Hole et al., 2000), determined in an active source seismic refraction survey. Only events within the bounds of the velocity model (east of −125°W and south of 41°N) were relocated and retained. We assigned velocities in a cubic lattice at nodes with horizontal and vertical spacings of 7 and 3 km, respectively and performed the relocation using the simul2000 algorithm (Evans et al., 1994). Velocities deeper than 27 km were set to a constant 8.55 km/s. At this step, 1,452 of the manually picked events were relocated and retained. The median root-mean-square misfit for the data set at this step was 0.16 s.

3.1.3. Relative Event Relocation

Relative locations were refined with the GrowClust algorithm (Trugman & Shearer, 2017). This method clusters events hierarchically then relocates them relatively using inter-event cross-correlation values and differential travel times. Unmodeled velocity perturbations and outliers are mitigated with this method. Since the algorithm minimizes against the L1 norm, it is less sensitive to outliers. We only cluster and relocate events that meet the criteria for cross-correlation (cc > 0.2 for event pair at common station) and distance (max station distance 200 km). At this step, 1,134 of the events were relocated and others retained their initial location (a final event count of 1,452). GrowClust uses the non-parametric resampling technique (Efron & Tibshirani, 1994) to estimate location uncertainties. The median horizontal and vertical errors are roughly 400 m. Our final locations are shown in Figure 1.

3.2. Template Matching Plate Interface Events

Events near the plate interface may be a probe into the stress state of the neighboring plate boundary. The focus of our study is earthquakes on or near the plate interface and their temporal behavior and potential relationship to other modes of slip on the interface. We use the high-quality locations to identify events that are within the approximate uncertainty (5 km) of the plate interface model from McCrory et al. (2012). There are 526 events that meet these criteria. Figure 2 shows events plotted in cross section, and most events near the interface are deeper than 15 km (see Figure S1 for a histogram showing the distribution of event depths that are within 5 km of the plate interface). Since we are interested in investigating the long-term temporal behavior of the interface region (beyond the limited 15-month duration of the CI deployment) we select only those events that have at least three P-phase arrivals on permanent NCSN seismic stations to perform template matching. Using three or more stations increases confidence that a template matched detected event has a similar location as the template. Two hundred events meet this requirement and serve as template waveforms for match filtering over continuous waveform data (a map showing template event locations is shown in Figure S2). Match filtering techniques exploit the fact that seismograms are a convolution of source, path, and receiver filters, and it follows that the seismograms of two events with similar location and faulting recorded at the same station will have a similar ray path, and thus similar waveforms and high inter-event cross correlation values. The plate interface template events help identify other nearby events over the timespan of January 2010–January 2020, allowing us to explore the temporal and evolution behavior of these plate interface events.

We carry out the template matching using the EQcorrscan python package which has the advantages and capabilities of parallelization, several quality control methods to limit spurious detections, and performs normalized multi-channel cross correlation over day-long waveform segments (Chamberlain et al., 2018). We preprocess all waveform data, templates, and continuous waveform data, by applying a zero-phase fourth order 3–10 Hz bandpass filter, down sampled to 25 Hz. The template events are trimmed to 0.15 s before the P-pick to a total duration of 4.6 s. Our criteria for detections are that the matched event must have an average cross-correlation coefficient greater than 0.6 and a median absolute deviation greater than 10. We set these criteria to ensure that templates and detections are nearby (Frémont & Malone, 1987; Geller & Mueller, 1980). In the template matching routine, we remove channels with spurious data-spikes as they will cause errors in the cross-correlation calculation. Following match filtering, the detection catalog is post-processed. We remove duplicate detections that occur when multiple templates match with the same detection and retain the detection with the highest inter-event cross-correlation value. Additionally, we

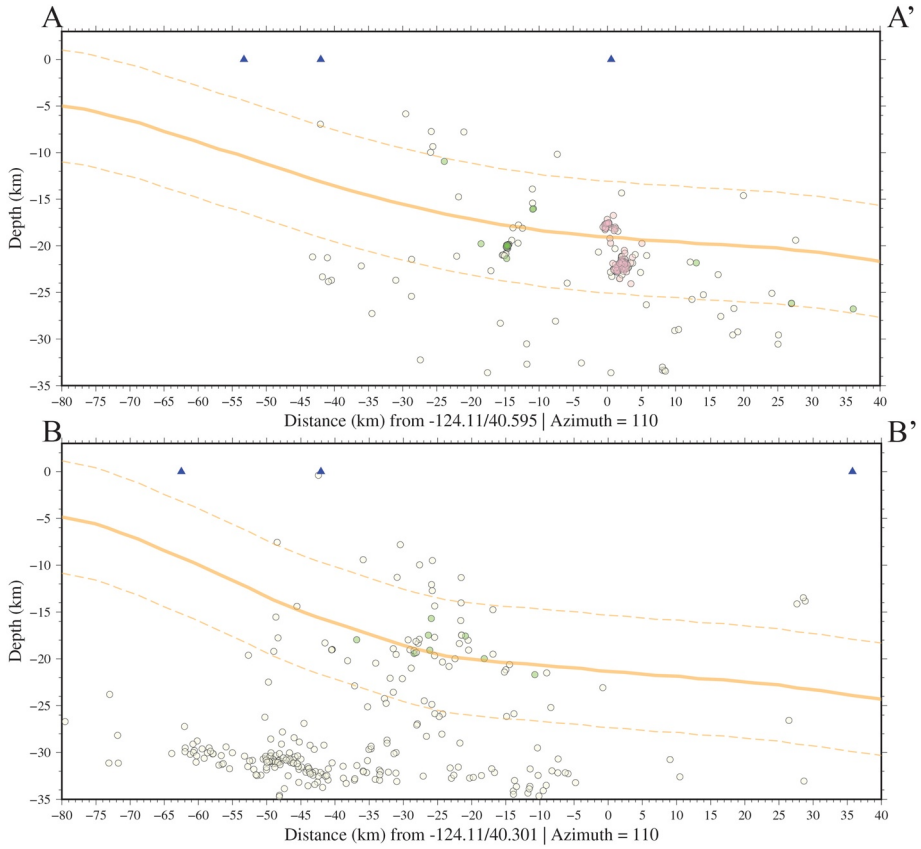

Figure 2. Cross sections as indicated in Figure 1. The solid yellow line indicates the location of the plate interface (McCrory et al., 2012). Dashed lines show ±5 km from the plate interface. Cross sections include all relocated events within 7 km of the cross section as open circles. Colored circles indicate template events that occur within the ±5 km around the interface that found matches, in match filtering. The pink circles denote events that were used for template matching of clusters of events located below temporary station CM04A that represent a significant fraction of interface events (Fortuna cluster). The green circles indicate other template events that found matches. A–A′ (top) B–B′ (bottom).

scan the catalog for detections that occur within 2 s of each other, again saving the event with the highest inter-event cross correlation value. See an example of detection and template in Figure 3.

Template matching of the 200 templates finds 2,363 unique detections over the time span of January 2010–January 2020 (see Figure S3 for a time series showing all detections). One thousand five hundred and nineteen of these detections are made with 106 templates that occur clustered below CI station CM04A near Fortuna, northern California (and clearly anomalous in Figure S4), while the remaining 94 plate interface template events identify 844 unique detections. There are roughly the same number of templates generated within the cluster as there are in aggregate around the remaining plate interface; however, the cluster templates identify nearly 2 times more detections. The cluster of events accounts for roughly 10% of our catalog's total number of events and is confined to a small volume ~3 km in radius (Figure 1) The cluster exhibits noteworthy temporal clustering as well. There were no detections prior to February 2013, and only a handful of events occurred before activity abruptly increased in February 2014 and continued for 2 years. This cluster of events, hereon referred to as the Fortuna cluster, is anomalous in temporal behavior and in the density of events in space. The Fortuna cluster's association with other plate interface observables are discussed in further detail in the Discussion section.

3.3. Determining Faulting Geometry

To discriminate interplate from intraplate events within the Fortuna cluster, we generate focal mechanisms. We employ the first motion polarity inversion method of HASH (Hardebeck & Shearer, 2002), which is a

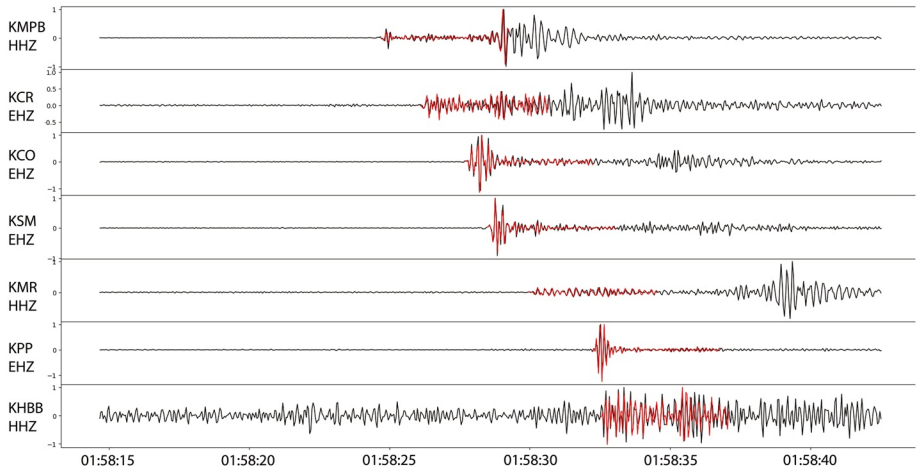

Figure 3. An example of template matching results. Template waveform shown in red overlain on detecting waveform in black. Amplitudes are normalized by their maximum. This match was detected on seven channels of permanent Northern California Seismic Network stations, the detection has an average cross correlation value of 0.9. The template event occurred on 2014-12-23 and this event was detected 2014-3-2, which is the approximate time that the Fortuna cluster initiates.

routine method of small mechanism determination and accounts for errors in location, velocity model, and possible polarity mis-picks. Here we specify a maximum azimuth gap of 90° and a minimum of 7 polarities to grid search for preferred double couple solutions. We presume that most of our polarities are accurate (0.05 polarity errors) due to manual inspection on all stations (CI & NCSN) in the snuffler—pyrocko package (Heimann et al., 2017), which allows for fine tuning filters actively while examining the waveforms, allowing us to ensure stability of the polarity from lower to higher frequencies. The magnitude of these events ranges from magnitude 0 to 3. Mechanisms were successfully calculated for 37 of the 106 template events, though we only interpret events that are "C" quality and better. We generate 8 C and 5 C and B quality mechanisms respectively, refer to Hardebeck and Shearer (2002) for a description of mechanism quality. Figure 4 shows a map with these event focal mechanisms. There is a diversity of faulting geometry with both strike slip and dip slip events occurring, and examples of each plotted with first motion arrivals on a stereonet can be found in Figure S5.

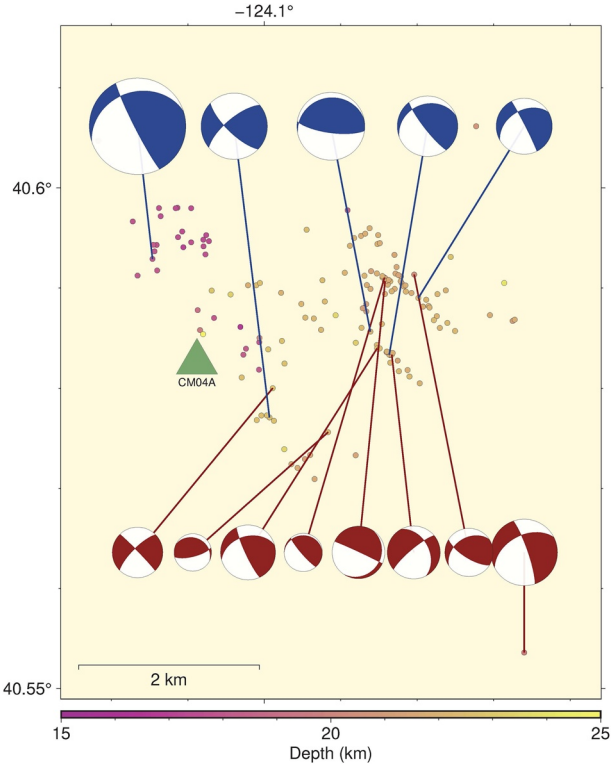

Figure 4. Zoom in of the Fortuna seismicity cluster (location indicated by yellow box in Figure 1). Focal mechanisms are first motion determined and inverted with HASH. Blue mechanisms indicate "B" Quality, Red are "C" quality. Also included are all relocated events in the area colored by depth.

4. Discussion

4.1. Comparison With Other Catalogs

We create a high-resolution catalog of 1,452 events to help identify earthquakes that occur near the plate interface, including smaller events not identified previously. Over the same time (July 2014–October 2015) and region (40°N to 41°N/−123°W– to −125°W) as this study, the NCSN high-quality double-difference catalog contains 446 events, and the Advanced National Seismic System (ANSS) catalog includes 552 events. We increased the number of identified events by a factor of 3 (Figure S6 for a comparison of the catalog from this study and ANSS catalog). Our catalog also improves the magnitude of completeness over the ANSS catalog from 1.75 to 1.5 (Figure S8). Completeness was calculated using the maximum curvature method. This newly created catalog is a clear improvement on the existing routinely generated catalogs.

This catalog is the first to fully include the year 4 densely spaced CI amphibious data. The events in our catalog were picked manually by human analysts and include low magnitude events (M_L 0–3.5) that are easily missed by automated methods. Our events are located with the best available 3D velocity model (Hole et al., 2000), and event locations are improved with cross-correlation based relative relocation methods. Chen and McGuire (2016) investigated seismicity in southern Cascadia using CI data; however, the data they used were from the September 2012 to February 2013 phase of the deployment which had much larger station spacing and did not include the additional land stations deployed in 2014. Using STA/LTA ratios the same 3D velocity model and TomoDD double difference relocation method they created a catalog of 1,137 earthquakes. Their area of investigation extended much further west and included many more events along the seismically active Mendocino Fracture Zone, which were not the focus of this study. Stone et al. (2018) used data from the complete 4-year duration of the Cascadia Initiative to explore the distribution of seismicity along the entire Cascadia Subduction Zone, though the study focused on latitudes north of 41°N, thus omitting southern Cascadia (40°N–41°N). Our newly generated catalog fills and complements the existing Cascadia Initiative experiment studies.

4.2. Seismicity Trends

Our high-resolution earthquake catalog illuminates many interesting seismicity features and trends. Diffuse clouds of seismicity generally relocate to tight and linear clusters (highlighted in Figure S7). Seismicity delineates the Mendocino Fracture Zone, which is partially creeping (Materna, et al., 2018). Relatively few events are located within the upper plate, and it is challenging to associate events with mapped USGS quaternary active faults. However, several of the events and linear features are consistent with the trend of many of the mapped quaternary faults (Figure S7).

Apart from the Mendocino Fracture Zone, other linear trends of seismicity are at depths consistent with occurring within the Gorda slab and are oriented sub-parallel to the trend of the San Andreas Fault, upper plate mapped active faults, and strike-slip faults on the incoming Gorda plate. The most notable of these features appears near the Mendocino Triple Junction in the Gorda slab as a continuous band of seismicity extending over 30 km in length (Figure S7). These events are observable in existing catalogs but as diffuse seismicity; here they clearly delineate a fault. Chen and McGuire (2016) also noticed this localized region of earthquakes and pointed out that events along this fault, within the oceanic mantle, had an order of magnitude higher stress drops than events located shallower near the plate interface. These trends of seismicity may be delineating a fabric within the Gorda slab that is also expressed in faulting in the upper plate.

There is a general absence of seismicity near the shallow interface (shallower than 15 km) during the period of investigation (Figure 2), indicating that the plate boundary is either highly coupled and accumulating strain or stably sliding. If the interface were stably sliding without earthquakes, it would require homogeneous velocity strengthening materials and no velocity weakening asperities, which has not been documented. Alternatively, the interface could have velocity weakening asperities that are too small in area or slip that the magnitude would be below the limits of our observations. Another possibility is that the shallow updip region is in a stress shadow of high coupling in the seismogenic zone below this depth and thus kinematically locked (Lindsey et al., 2021). While we acknowledge that the shallow region could be sliding completely aseismically, we favor locking because the configuration of the seismic array provided excellent coverage offshore and maximum detectability of events and a thorough examination shows extremely sparse seismicity. The probable high coupling of the megathrust from the trench to the downdip limit of locking has implications for earthquake and tsunami modeling efforts. The larger area of locking implies that there is a larger area accumulating strain and a larger impending rupture area, and thus a larger magnitude than if this updip area was less coupled and creeping. Additionally, if the toe of the subduction zone is accumulating strain, then more shallow slip will occur and displace a greater volume of the overlying ocean, exciting a larger tsunami (Lay et al., 2019).

Although the shallowest portion of the megathrust is mostly devoid of seismicity, there are 526 events that are located within 5 km of the plate interface. These near plate interface events are small with magnitudes between 0 and 3.4, the mean magnitude for these events is 1.2 ± 0.6. Most events near the plate interface occur deeper than 15 km, with a mean depth of 20.8 ± 3.2 km (see Figure S1). The depth of the majority of the near plate interface events coincides with the transition from a high to low coupled plate interface at

about 20 km (the lower limit of the seismogenic zone) (Hyndman, 2013; Schmalzle et al., 2014), as well as shallowing of the dip of the plate interface (see interface contours on Figure 1). The most noteworthy near plate interface events occur in the Fortuna cluster of 146 earthquakes, which is 10% of the entire catalog, located at 40.6 N/124.1 W, 20 km beneath Fortuna, California (yellow box in Figure 1). This cluster accounts for a significant fraction of the seismicity in the study area and is spatially concentrated, confined to an $\sim$30 km^2 area.

4.3. Fortuna Earthquake Cluster

The Fortuna cluster is located directly beneath the temporary CI station CM04A, near the interface. Locations are well determined due to the dense station spacing and good azimuthal coverage in this area. The events appear to form two distinct clusters, one centered at a depth of 17 km and the other at 22 km depth (Figure 2a). To determine if this cluster is unique in time, we examined seismicity in the area from the ANSS catalog over the last 40 years from 1980 to 2020 (Figure 5). This cluster of seismicity is clearly visible in the ANSS catalog only during the 2014–2015 time period (indicated in Figure 5a). A closer examination of the volume surrounding this cluster reveals that it may have had a burst of seismicity toward the end of 1982 (Figure 5b) but is quiet at all other times. The cluster straddles the plate interface (pink circles in Figure 2) of McCrory et al., 2012. The event locations and depths are consistent with the proposed downdip limit of high coupling in Cascadia (Hyndman, 2013; Schmalzle et al., 2014). Near this cluster, the McCrory slab morphology is unusual, dipping concave up rather than continuous concave down geometry observed elsewhere along the Cascadia margin.

There is a diversity of faulting geometry for well-constrained focal mechanisms in this cluster, in that there are both strike-slip and dip-slip earthquakes (Figure 4). The strike-slip mechanisms are oriented similarly to large strike-slip earthquakes that have been observed in the incoming Gorda plate (Chaytor et al., 2004; Gulick et al., 2001) and oriented sub-parallel to the strike of the San Andreas Fault, suggesting a reactivation of a preexisting structure or merely response to the regional stresses. The thrust focal mechanisms are consistent with the relative plate motion between the subducting and overriding plates. The variety of focal mechanisms leads to tenuous seismotectonic conclusions. However, the complexity of focal mechanisms indicates that these events do not occur on a single fault with a consistent sense of motion; they do not represent rupture of a single repeating asperity. The diversity of focal mechanisms indicates that the events are responding to a complex regional stress field and possibly reactivation of a pre-existing fabric.

Magnitudes of events within this cluster are between 0 and 3.5, and events do not show a clear mainshock-aftershock magnitude distribution nor an Omori like aftershock sequence (Figure 5c), suggesting swarmogenic behavior (Mogi, 1963; Nishikawa & Ide, 2017; Vidale & Shearer, 2006). Our catalog reveals that the duration of this cluster is several years (2014–2017, Figure 6) which is longer than swarm activity occurring in other regions. Swarms have been reported to typically last on the order of weeks to a few months (Lohman & McGuire, 2007; Miller et al., 2004; Roland & McGuire, 2009; Vidale & Shearer, 2006; Xue et al., 2018). However, recently a long-lived swarm, $\sim$4 years in duration, has been documented in southern California (Ross et al., 2020) that is closer to the duration of the persistent activity in this study. The swarm in Ross et al. (2020) exhibits a clear expanding migratory pattern that is inferred to be fluid driven and structurally guided. Our study differs vastly in that we have identified many fewer events and only weak northwest to southeast migratory behavior (Figure S9). Cascadia does not have any documented tectonic swarm activity (Holtkamp & Brudzinski, 2011; Nishikawa & Ide, 2017). The long duration of activity, absence of clear fluid induced migration, and lack of spatio-temporal correlation with documented slow slip events make us hesitant to classify the localized seismicity here as a swarm. Instead, we prefer to refer to it as a seismicity cluster. Another example of an isolated seismicity cluster in space and time was recently documented in northern Cascadia. Merrill and Bostock (2019) identified an earthquake nest located in the Juan de Fuca mantle at depths greater than 60 km and concentrated in a $30 \times 10 \times 10$ km^3 volume. Generally, nests are classified as intraslab intermediate depth seismicity that persists for decades (Prieto et al., 2012). Our cluster is confined to a $\sim 6 \times 6 \times 6$ km^3 region with depths between 17 and 23 km, therefore it does not fit the definition of an earthquake nest. The proximity of this locus of events to the plate interface suggests that it is likely experiencing a similar stressing field as the plate interface.

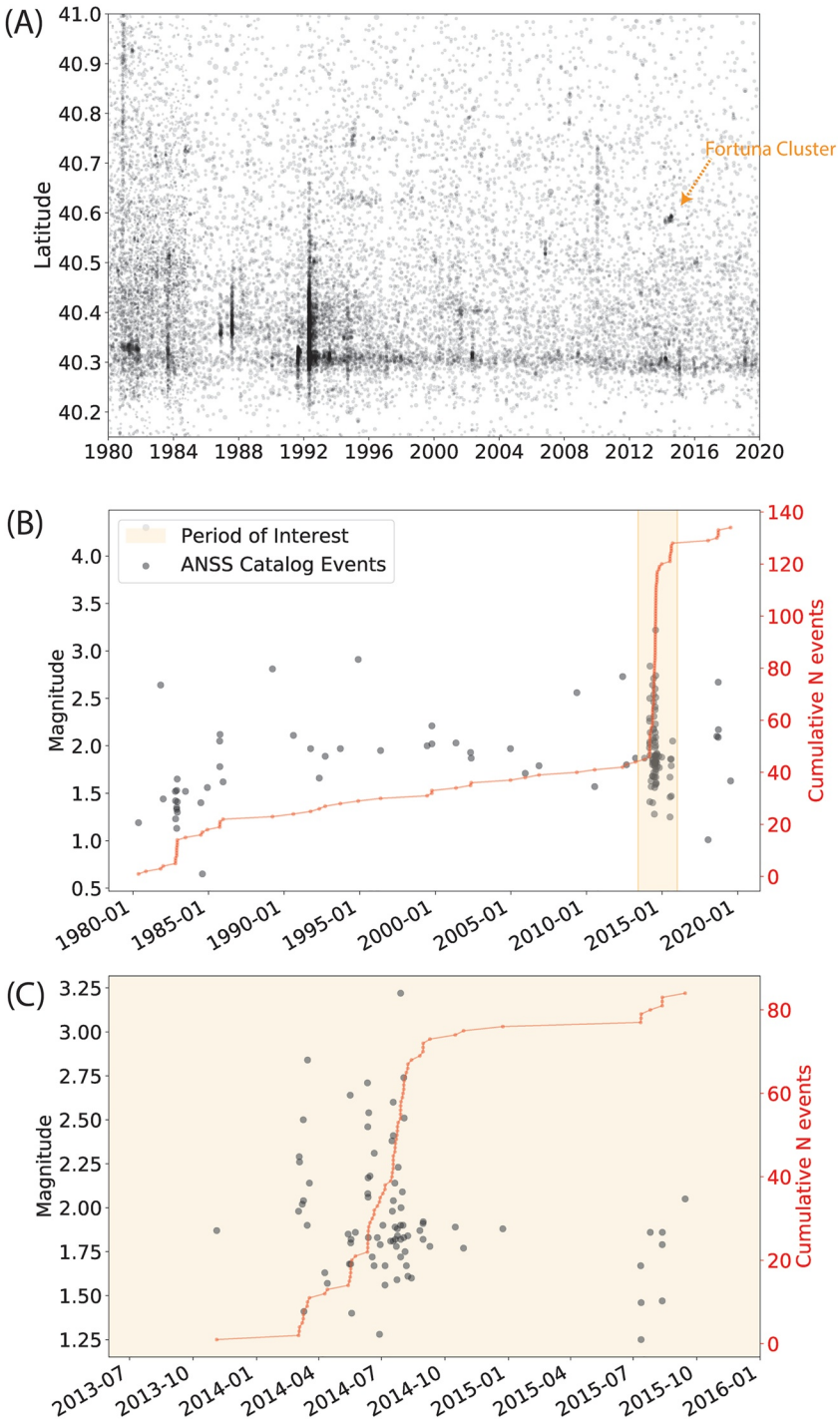

Figure 5. (a) Advanced National Seismic System (ANSS) comcat catalog over the bounds of the study area 40°N to 41°N/125°W to 123°W, showing event latitude as a function of time. Fortuna cluster (40.6°N) clearly anomalous in 2014. (b) Plot showing events from ANSS 1980–2020 activity in 10 × 10 × 10 km^3 volume centered on Fortuna cluster (40.6°N/123.1°W/20 km depth). Note the sparse activity prior to 2014, which drastically increased starting March 2, 2014, which is shown clearly on the (c) plot.

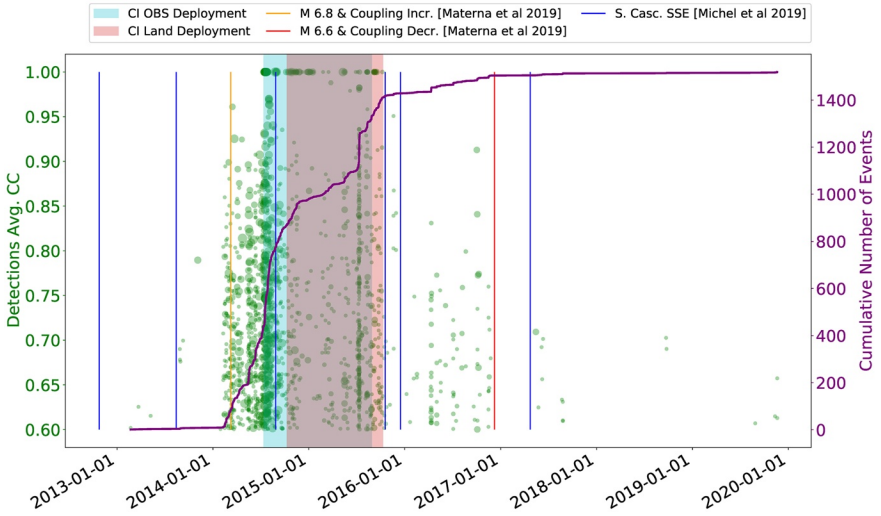

Figure 6. Time series showing template matched detections for templates in the Fortuna cluster. Template matching was performed over the time period of January 2010 through January 2020; the first detection occurred in February 2013, and detections increased significantly in February 2014. There were 106 template events used here to identify 1,519 unique detected events. The green markers are detections where marker size is scaled by the number of channels used in detections, ranging from 3 to 11 channels, smallest to largest respectively. The events with cross-correlation values = 1 are templates finding themselves in continuous data. Purple curve shows the cumulative number of detections. Blue vertical lines indicate the approximate timing of maximum moment of Southern Cascadia slow slip events from Michel et al., 2019. Yellow and red vertical lines indicate the timing of large regional earthquakes (Figure 1) and approximate timing of long-term strain transient from Materna et al. (2019). Light blue region highlights Cascadia Initiative (CI) ocean bottom seismometers deployment, light pink region highlights CI land deployment, and the purple area is the overlap of both data sets.

4.4. Fortuna Cluster and Strain Transients

Template matching of the 106 events within the Fortuna cluster over the timespan of 2010–2020 identifies over 1,500 newly detected events (Figure 6). Most of these new detections are concentrated in time. This confirms the finding of the ANSS comprehensive catalog (Figure 5c) that the cluster region was primarily active during a short interval of time around 2014–2016 with little to no seismic activity outside of this period. The timing of this near-interface seismicity does not appear to correlate with southern-Cascadia slow slip events (Figure 6) that occur down-dip of this cluster (Michel et al., 2019); suggesting that the cluster is not sensitive to or driven by downdip slow slip events.

There is a temporal correlation between the Fortuna cluster and long-term regional strain transients (Figure 6) (Haines et al., 2019; Materna et al., 2019; Nuyen & Schmidt, 2021). Materna et al. (2019) and Nuyen and Schmidt (2021) identified two abrupt velocity changes (early 2014 and early 2017) in the southern Cascadia GNSS time series. They modeled these velocity changes as variations in slip on the megathrust at a depth of ~30 km in the gap between the ETS zone and the downdip limit of the highly coupled zone (Gao & Wang, 2017), ~40 km from the Fortuna cluster. These changes bracket the time that the Fortuna seismicity cluster is active, and seismicity rate rapidly increases in February 2014. Nuyen and Schmidt (2021) propose that the 2014 GNSS velocity change was the rapid arrest of a long-term slow slip event, which started in mid-2012. Alternatively, Materna et al. (2019) attribute the 2014 regional GNSS velocity change to a dynamically triggered increase in megathrust coupling occurring in response to the March 10, 2014, M 6.8 offshore strike-slip earthquake (Figure 1). Before the 2014 earthquake, Materna et al. (2019) observe steady velocities. Materna et al. (2019) speculate that the 2014 velocity change occurs as fluids are liberated from the region in response to the passage of seismic waves that reduces pore-pressure and increases effective normal stresses, decreasing the ability of the plate interface to slide stably (Figure 7). The most substantial GNSS velocity change occurs in early 2014 and reflects either an increase in coupling or the termination of the 1.5-year long-term slow slip event. A more recent long-term strain transient occurred near the end of 2016 and beginning of 2017, indicated by a reduced eastward velocity and interpreted as a decrease of coupling on the plate interface (Materna et al., 2019) or the onset of a long-term slow slip event (Nuyen &

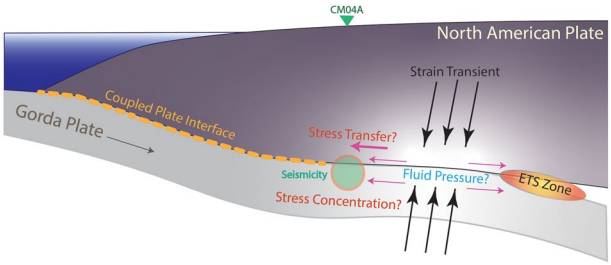

Figure 7. Cartoon schematic cross section representation of observations described in the discussion section. Region of strain transient (coupling increase or the termination of a long-term slow slip event) is intermediate between the downdip limit of locking and the episodic tremor and slip region. Seismicity clustered near the downdip limit of locking is activated contemporaneously with the strain transient. The two observations are temporally correlated and we speculate that the cluster is the seismic manifestation of the strain transient. Also shown is the coupled region of the plate interface extending all the way to the trench, which is suggested by the lack of plate interface seismicity. Modified after Materna et al., 2019.

Schmidt, 2021). This motion change also conspicuously coincides with a large M 6.6 regional earthquake on December 8, 2016 on the Mendocino Fracture Zone (Figure 1). As with the previous strain transient, Materna et al. (2019) speculate that this has occurred in response to dynamic triggering by a large regional earthquake. This velocity change occurs as the Fortuna cluster seismicity rate decreases.

Since the Fortuna seismicity cluster is unique in time and temporally correlated with GNSS strain transient observations, we surmise that the two observations are related and that we can therefore obtain better temporal resolution of the long-term strain transient using the onset time of the seismicity cluster. The cluster suddenly initiates about one month before the 2014 M 6.8 earthquake and continues through early 2017, at which time Fortuna cluster seismicity terminates (Figure 6). An abrupt strain transient on nearby borehole strainmeter stations B045 and B933 (locations shown in Figure 1) occurs in February 2014 when the seismicity cluster initiates (Figure S10) and supports that the onset of the 2014 strain transient precedes the M 6.8 2014 earthquake. However, exactly how the Fortuna seismicity cluster and increased eastward motion relates to the strainmeter transient is unclear from only two strainmeter observations.

What is clear is that the Fortuna seismicity cluster occurs on and close to the megathrust in a region of slab distortion that is sensitive to plate interface stress perturbations. It is uniquely bracketed in time by a period of increased eastward GNSS velocity, attributed to a period of increased locking or between long-term slow slip events. The diversity in faulting geometry suggests that this cluster occurs in a region of a stress concentration. Although we cannot conclusively determine the Fortuna cluster's driving mechanism, it is likely either driven by fluids liberated from the region of coupling increase or by stress transfer attributed to relocking following a long-term slow slip event (Figure 7). In either case, the Fortuna cluster appears related to and may indicate the long-term plate interface strain transients. Similar to the way tremor is used as a timing proxy for slow slip events, earthquake clusters may be useful as a timing proxy for coupling changes and provide further insight into the range of plate interface behavior.

5. Conclusions

We construct a 15 month (July 2014–October 2015) high resolution earthquake catalog for the southernmost Cascadia margin near the Mendocino Triple Junction. This catalog demonstrates a clear lack of seismicity in the shallow updip plate interface region. This absence of seismicity along the shallow interface suggests that the interface is highly coupled. We also observe a cluster of events that locates near a contortion in the plate interface at the downdip limit of the highly coupled seismogenic zone. Using template matching, we investigate this cluster's activity during the extended period between 2010 and 2020. We detect over 1,500 events that occur within a 3-year period (2014–2017) bracketed in time by an abrupt GNSS increase in eastward velocity that has been interpreted as a coupling increase, or between long-term slow slip events. We speculate that the seismicity is a response to the strain transient on the interface, as either a result of stress transfer reactivating pre-existing fabrics or fluid migration and can therefore provide constrains on the onset and termination time. This is particularly useful since the precise timing of the long-term strain transients are not well determined from the GNSS time series. We propose that seismicity clusters may be used to help delineate the onset and termination of long-term changes in plate interface slip behavior.

Data Availability Statement

Raw data can be obtained from the IRIS Data Management Center at https://ds.iris.edu/mda/7D/?starttime=2011-01-01T00:00:00&endtime=2017-12-31T00:00:00, https://ds.iris.edu/mda/5E/?starttime=2014-01-01T00:00:00&endtime=2015-12-31T00:00:00, https://ds.iris.edu/mda/NC/ (last accessed August 2019). The relocated catalog generated in this study is available in Data Set S1.

Acknowledgments
We thank the Cascadia Initiative Expedition Team for their dedication to creating a large scale community experiment and making the data used in this study widely available. The authors wish to thank two anonymous reviewers who helped to improve the content and clarity of the manuscript. We acknowledge the helpful contribution of the UC Santa Cruz COSMOS students, Iris Xia and Flora Huang for assistance with P-phase picks. This work benefited from helpful discussions with members of the UC Santa Cruz seismology laboratory. Seismograms used in this study were collected as part of the Cascadia Initiative Experiment using onshore seismometers operated by IRIS and ocean bottom seismometers from OBSIP. This material is based on work partial funded by the National Science Foundation (EAR-1551683).

References

Bartlow, N. M. (2020). A long-term view of Episodic tremor and slip in Cascadia. *Geophysical Research Letters*, *47*(3), e2019GL085303. https://doi.org/10.1029/2019GL085303

Bartlow, N. M., Miyazaki, S., Bradley, A. M., & Segall, P. (2011). Space-time correlation of slip and tremor during the 2009 Cascadia slow slip event. *Geophysical Research Letters*, *38*(18), L18309. https://doi.org/10.1029/2011GL048714

Bilek, S. L., Lay, T., and Ruff, L. J. (2004). Radiated seismic energy and earthquake source duration variations from teleseismic source time functions for shallow subduction zone thrust earthquakes. *Journal of Geophysical Research*, *109*(B9), B09308. https://doi.org/10.1029/2004JB003039

Brudzinski, M. R., & Allen, R. M. (2007). Segmentation in episodic tremor and slip all along Cascadia. *Geology*, *35*(10), 907. https://doi.org/10.1130/g23740a.1

Bürgmann, R. (2018). The geophysics, geology and mechanics of slow fault slip. *Earth and Planetary Science Letters*, *495*, 112–134. https://doi.org/10.1016/j.epsl.2018.04.062

Chamberlain, C. J., Hopp, C. J., Boese, C. M., Warren-Smith, E., Chambers, D., Chu, S. X., et al. (2018). EQcorrscan: Repeating and Near-Repeating Earthquake Detection and Analysis in Python. *Seismological Research Letters*, *89*(1), 173–181. https://doi.org/10.1785/0220170151

Chaytor, J. D., Goldfinger, C., Dziak, R. P., & Fox, C. G. (2004). Active deformation of the Gorda plate: Constraining deformation models with new geophysical data. *Geology*, *32*(4), 353–356. https://doi.org/10.1130/G20178.2

Chen, X., & McGuire, J. J. (2016). Measuring earthquake source parameters in the Mendocino triple junction region using a dense OBS array: Implications for fault strength variations. *Earth and Planetary Science Letters*, *453*, 276–287. https://doi.org/10.1016/j.epsl.2016.08.022

DeMets, C., Gordon, R. G., Argus, D. F. (2010). Geologically current plate motions. *Geophysical Journal International*, *181*, 1–80. https://doi.org/10.1111/j.1365-246X.2009.04491.x

Dieterich, J. (1994). A constitutive law for rate of earthquake production and its application to earthquake clustering. *Journal of Geophysical Research*, *99*(B2), 2601–2618. https://doi.org/10.1029/93jb02581

Dieterich, J. H. (1986). A model for the nucleation of earthquake slip. In Earthquake Source Mechanics, 37, 37–47. https://doi.org/10.1029/GM037p0037

Dragert, H. (2001). A silent slip event on the deeper Cascadia subduction interface. *Science*, *292*(5521), 1525–1528. https://doi.org/10.1126/science.1060152

Efron, B., & Tibshirani, R. J. (1994). *An introduction to the bootstrap*. CRC press.

Evans, J. R., Eberhart-Phillips, D., & Thurber, C. H. (1994). *User's manual for SIMULPS12 for imaging Vp and Vp/Vs; a derivative of the" Thurber" tomographic inversion SIMUL3 for local earthquakes and explosions (No. 94–431)*. US Geological Survey.

Frank, W. B., & Brodsky, E. E. (2019). Daily measurement of slow slip from low-frequency earthquakes is consistent with ordinary earthquake scaling. *Science Advances*, *5*(10), eaaw9386. https://doi.org/10.1126/sciadv.aaw9386

Frémont, M.-J., & Malone, S. D. (1987). High precision relative locations of earthquakes at Mount St. Helens, Washington. *Journal of Geophysical Research*, *92*(B10), 10223–10236. https://doi.org/10.1029/JB092iB10p10223

Gao, X., & Wang, K. (2017). Rheological separation of the megathrust seismogenic zone and episodic tremor and slip. *Nature*, *543*(7645), 416–419. https://doi.org/10.1038/nature21389

Geller, R. J., & Mueller, C. S. (1980). Four similar earthquakes in central California. *Geophysical Research Letters*, *7*(10), 821–824. https://doi.org/10.1029/GL007i010p00821

Gulick, S. P. S., Meltzer, A. S., Henstock, T. J., & Levander, A. (2001). Internal deformation of the southern Gorda plate: Fragmentation of a weak plate near the Mendocino triple junction. *Geology*, *29*(8), 691. https://doi.org/10.1130/0091-7613(2001)029<0691:IDOTSG>2.0.CO;2

Haines, J., Wallace, L. M., & Dimitrova, L. (2019). Slow slip event detection in Cascadia using vertical derivatives of horizontal stress rates. *Journal of Geophysical Research: Solid Earth*, *124*, 5153–5173. https://doi.org/10.1029/2018JB016898

Hardebeck, J. L., & Shearer, P. M. (2002). A new method for determining first-motion focal mechanisms. *Bulletin of the Seismological Society of America*, *92*, 2264–2276. https://doi.org/10.1785/0120010200

Heimann, S., Kriegerowski, M., Isken, M., Cesca, S., Daout, S., Grigoli, F., et al. (2017). *Pyrocko - An open-source seismology toolbox and library. V. 0.3*. GFZ Data Services. https://doi.org/10.5880/GFZ.2.1.2017.00

Hole, J. A., Beaudoin, B. C., & Klemperer, S. L. (2000). Vertical extent of the newborn San Andreas fault at the Mendocino triple junction. *Geology*, *28*(12), 1111–1114. https://doi.org/10.1130/0091-7613(2000)028<1111:veotns>2.3.co;2

Holtkamp, S. G., & Brudzinski, M. R. (2011). Earthquake swarms in circum-Pacific subduction zones. *Earth and Planetary Science Letters*, *305*(1–2), 215–225. https://doi.org/10.1016/j.epsl.2011.03.004

Hyndman, R. D. (2013). Downdip landward limit of Cascadia great earthquake rupture. *Journal of Geophysical Research: Solid Earth 118*, 5530–5549. https://doi.org/10.1002/jgrb.50390

Igarashi, T., Matsuzawa, T., & Hasegawa, A. (2003). Repeating earthquakes and interplate aseismic slip in the northeastern Japan subduction zone. *Journal of Geophysical Research*, *108*(B5), 2249. https://doi.org/10.1029/2002JB001920

Lapusta, N., & Rice, J. R. (2003). Nucleation and early seismic propagation of small and large events in a crustal earthquake model. *Journal of Geophysical Research*, *108*(B4), 2205. https://doi.org/10.1029/2001JB000793

Lay, T., Kanamori, H., Ammon, C. J., Koper, K. D., Hutko, A. R., Ye, L., & Rushing, T. M. (2012). Depth-varying rupture properties of subduction zone megathrust faults. *Journal of Geophysical Research*, *117*(B4), B04311. https://doi.org/10.1029/2011jb009133

Lay, T., Liu, C., Kanamori, H., 2019. Enhancing tsunami warning using *P* wave coda. *Journal of Geophysical Research: Solid Earth*, *124*, 10583–10609. https://doi.org/10.1029/2019JB018221

Li, S., Wang, K., Wang, Y., Jiang, Y., & Dosso, S. E. (2018). Geodetically inferred locking state of the Cascadia megathrust based on a viscoelastic Earth model. *Journal of Geophysical Research: Solid Earth*, *123*(9), 8056–8072. https://doi.org/10.1029/2018JB015620

Lindsey, E. O., Mallick, R., Hubbard, J. A., Bradley, K. E., Almeida, R. V., Moore, J. D. P., et al. (2021). Slip rate deficit and earthquake potential on shallow megathrusts. *Nature Geoscience*, *14*(5), 321–326. https://doi.org/10.1038/s41561-021-00736-x

Lohman, R. B., & McGuire, J. J. (2007). Earthquake swarms driven by aseismic creep in the Salton Trough, California. *Journal of Geophysical Research*, *112*(B4), B04405. https://doi.org/10.1029/2006JB004596

Materna, K., Bartlow, N., Wech, A., Williams, C., & Bürgmann, R. (2019). Dynamically triggered changes of plate interface coupling in southern Cascadia. *Geophysical Research Letters*, *46*(22), 12890–12899. https://doi.org/10.1029/2019GL084395

Materna, K., Taira, T., & Bürgmann, R. (2018). Aseismic transform fault slip at the Mendocino Triple Junction from characteristically repeating earthquakes. *Geophysical Research Letters*, *45*(2), 699–707. https://doi.org/10.1002/2017GL075899

McCaffrey, R., Qamar, A. I., King, R. W., Wells, R., Khazaradze, G., Williams, C. A., et al. (2007). Fault locking, block rotation and crustal deformation in the Pacific Northwest. *Geophysical Journal International*, *169*(3), 1315–1340. https://doi.org/10.1111/j.1365-246X.2007.03371.x
McCrory, P. A., Blair, J. L., Waldhauser, F., & Oppenheimer, D. H. (2012). Juan de Fuca slab geometry and its relation to Wadati-Benioff zone seismicity. *Journal of Geophysical Research*, *117*(B9), B09306. https://doi.org/10.1029/2012JB009407
Merrill, R., & Bostock, M. (2019). An earthquake nest in Cascadia. *Bulletin of the Seismological Society of America*, *109*(5), 2021–2035. https://doi.org/10.1785/0120190055
Michel, S., Gualandi, A., & Avouac, J.-P. (2019). Interseismic coupling and slow slip events on the Cascadia megathrust. *Pure and Applied Geophysics*, *176*(9), 3867–3891. https://doi.org/10.1007/s00024-018-1991-x
Miller, S. A., Collettini, C., Chiaraluce, L., Cocco, M., Barchi, M., & Kaus, B. J. P. (2004). Aftershocks driven by a high-pressure CO_2 source at depth. *Nature*, *427*(6976), 724–727. https://doi.org/10.1038/nature02251
Mogi, K. (1963). Some discussions on aftershocks, foreshocks and earthquake swarms: The fracture of a semi-infinite body caused by an inner stress origin and its relation to the earthquake phenomena (third paper). 東京大學地震研究所彙報 = Bulletin of the Earthquake Research Institute, University of Tokyo, 41(3), 615-658.
Nadeau, R. M., & McEvilly, T. V. (2004). Periodic pulsing of characteristic microearthquakes on the San Andreas Fault. *Science*, *303*(5655), 220–222. https://doi.org/10.1126/science.1090353
Nishikawa, T., & Ide, S. (2017). Detection of earthquake swarms at subduction zones globally: Insights into tectonic controls on swarm activity. *Journal of Geophysical Research: Solid Earth*, *122*(7), 5325–5343. https://doi.org/10.1002/2017JB014188
Nuyen, C., & Schmidt, D. A. (2021). Filling the gap in Cascadia: The emergence of low-amplitude long-term slow slip. *Geochemistry, Geophysics, Geosystems*, *22*, e2020GC009477. https://doi.org/10.1029/2020GC009477
Pavlis, G. L., Vernon, F., Harvey, D., & Quinlan, D. (2004). The generalized earthquake-location (GENLOC) package: An earthquake-location library. *Computers & Geosciences*, *30*(9–10), 1079–1091. https://doi.org/10.1016/j.cageo.2004.06.010
Pollitz, F. F., & Evans, E. L. (2017). Implications of the earthquake cycle for inferring fault locking on the Cascadia megathrust. *Geophysical Journal International*, *209*. https://doi.org/10.1093/gji/ggx009
Prieto, G. A., Beroza, G. C., Barrett, S. A., López, G. A., & Florez, M. (2012). Earthquake nests as natural laboratories for the study of intermediate-depth earthquake mechanics. *Tectonophysics*, *570–571*, 42–56. https://doi.org/10.1016/j.tecto.2012.07.019
Roland, E., & McGuire, J. J. (2009). Earthquake swarms on transform faults. *Geophysical Journal International*, *178*(3), 1677–1690. https://doi.org/10.1111/j.1365-246X.2009.04214.x
Ross, Z. E., Cochran, E. S., Trugman, D. T., & Smith, J. D. (2020). 3D fault architecture controls the dynamism of earthquake swarms. *Science*, *368*(6497), 1357–1361. https://doi.org/10.1126/science.abb0779
Rouet-Leduc, B., Hulbert, C., & Johnson, P. A. (2019). Continuous chatter of the Cascadia subduction zone revealed by machine learning. *Nature Geoscience*, *12*(1), 75–79. https://doi.org/10.1038/s41561-018-0274-6
Satake, K., Wang, K., & Atwater, B. F. (2003). Fault slip and seismic moment of the 1700 Cascadia earthquake inferred from Japanese tsunami descriptions. *Journal of Geophysical Research*, *108*(B11), 2535. https://doi.org/10.1029/2003JB002521
Schmalzle, G. M., McCaffrey, R., & Creager, K. C. (2014). Central Cascadia subduction zone creep. *Geochemistry, Geophysics, Geosystems*, *15*(4), 1515–1532. https://doi.org/10.1002/2013GC005172
Schwartz, S. Y., & Rokosky, J. M. (2007). Slow slip events and seismic tremor at circum-Pacific subduction zones. *Reviews of Geophysics*, *45*(3), RG3004. https://doi.org/10.1029/2006RG000208
Segall, P., & Bradley, A. M. (2012). Slow-slip evolves into megathrust earthquakes in 2D numerical simulations. *Geophysical Research Letters*, *39*(18), L18308. https://doi.org/10.1029/2012gl052811
Shaddox, H. R., & Schwartz, S. Y. (2019). Subducted seamount diverts shallow slow slip to the forearc of the northern Hikurangi subduction zone, New Zealand. *Geology*, *47*(5), 415–418. https://doi.org/10.1130/G45810.1
Shelly, D. R., Beroza, G. C., & Ide, S. (2007). Non-volcanic tremor and low-frequency earthquake swarms. *Nature*, *446*(7133), 305–307. https://doi.org/10.1038/nature05666
Stone, I., Vidale, J. E., Han, S., & Roland, E. (2018). Catalog of offshore seismicity in Cascadia: Insights into the regional distribution of microseismicity and its relation to subduction processes. *Journal of Geophysical Research: Solid Earth*, *123*(1), 641–652. https://doi.org/10.1002/2017JB014966
Toomey, D., Allen, R., Barclay, A., Bell, S., Bromirski, P., Carlson, R., et al. (2014). The Cascadia Initiative: A sea change in seismological studies of subduction zones. *Oceanography*, *27*(2), 138–150. https://doi.org/10.5670/oceanog.2014.49
Trugman, D. T., & Shearer, P. M. (2017). GrowClust: A hierarchical clustering algorithm for relative earthquake relocation, with application to the Spanish Springs and Sheldon, Nevada, earthquake sequences. *Seismological Research Letters*, *88*(2A), 379–391. https://doi.org/10.1785/0220160188
Uchida, N., Takagi, R., Asano, Y., & Obara, K. (2020). Migration of shallow and deep slow earthquakes toward the locked segment of the Nankai megathrust. *Earth and Planetary Science Letters*, *531*, 115986. https://doi.org/10.1016/j.epsl.2019.115986
Vidale, J. E., & Shearer, P. M. (2006). A survey of 71 earthquake bursts across southern California: Exploring the role of pore fluid pressure fluctuations and aseismic slip as drivers. *Journal of Geophysical Research*, *111*(B5), B05312. https://doi.org/10.1029/2005JB004034
Walter, J. I., Schwartz, S. Y., Protti, M., & Gonzalez, V. (2013). The synchronous occurrence of shallow tremor and very low frequency earthquakes offshore of the Nicoya Peninsula, Costa Rica. *Geophysical Research Letters*, *40*(8), 1517–1522. https://doi.org/10.1002/grl.50213
Walton, M. A. L., Staisch, L. M., Dura, T., Pearl, J. K., Sherrod, B., Gomberg, J., et al. (2021). Toward an integrative geological and geophysical view of Cascadia subduction zone earthquakes. *Annual Review of Earth and Planetary Sciences*, *49*(1), 367–398. https://doi.org/10.1146/annurev-earth-071620-065605
Wang, K., & Tréhu, A. M. (2016). Invited review paper: Some outstanding issues in the study of great megathrust earthquakes—The Cascadia example. *Journal of Geodynamics*, *98*, 1–18. https://doi.org/10.1016/j.jog.2016.03.010
Xue, L., Bürgmann, R., Shelly, D. R., Johnson, C. W., & Taira, T. (2018). Kinematics of the 2015 San Ramon, California earthquake swarm: Implications for fault zone structure and driving mechanisms. *Earth and Planetary Science Letters*, *489*, 135–144. https://doi.org/10.1016/j.epsl.2018.02.018